Dalton Transactions

Accepted Manuscript

ROYAL SOCIETY OF CHEMISTRY

www.rsc.org/dalton

TABLE OF CONTENTS ENTRY

Different Topologies in Manganese-μ-Azido 1D Compounds: Crystal Structure, Magnetic Behavior, periodic DFT calculations and Quantum Monte Carlo simulations.

Franz A. Mautner, Christian Berger, Michael Scherzer, Roland C. Fischer, Lindley Maxwell, Eliseo Ruiz, Ramon Vicente.

Three new monodimensional azido-bridged manganese(II) complexes with general formula $[Mn(N_3)_2(L)_2]$ and different topologies are reported. Their magnetic properties have been studied. Periodic DFT calculations were performed to estimate the J values and Quantum Monte Carlo simulations were carried out using the calculated J values to check their accuracy in comparison with the experimental magnetic measurements.

Artwork

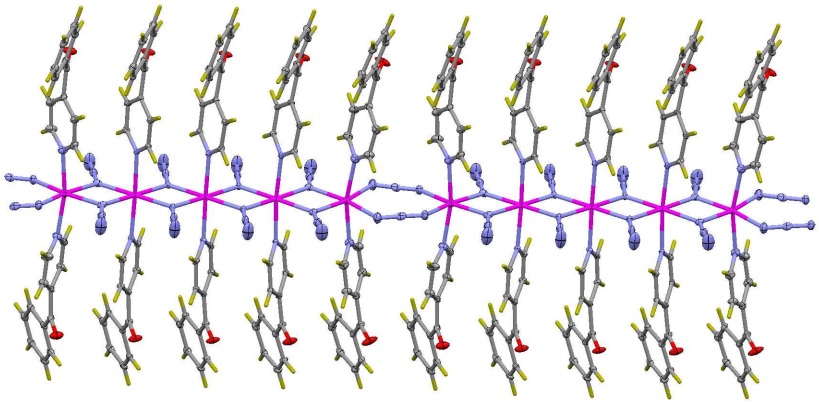

Different Topologies in Manganese-μ-Azido 1D Compounds: Crystal Structure, Magnetic Behavior, periodic DFT calculations and Quantum Monte Carlo simulations.[1]

Franz A. Mautner,[a] Christian Berger,[a]. Michael Scherzer,[a] Roland C. Fischer,[b] Lindley Maxwell,[c] Eliseo Ruiz,[c] Ramon Vicente.[d*]

[a] Institut für Physikalische and Theoretische Chemie, Technische Universität Graz, Stremayrgasse 9, A-8010 Graz, Austria

[b] Institut für Anorganische Chemie, Technische Universität Graz, Stremayrgasse 9, A-8010 Graz, Austria

[c] Departament de Química Inorgànica and Institut de Química Teòrica i Computacional (IQTC). Diagonal 645, 08028, Barcelona, Spain.

[d] Departament de Química Inorgànica and Institut de Nanociència i Nanotecnologia de la Universitat de Barcelona (IN^{2}UB). Martí i Franqués 1-11, 08028, Barcelona, Spain. Fax: +34 93490 7725; E-mail: ramon.vicente@qi.ub.es; FAX: ++34934907725

Abstract.

The syntheses and structural characterization of three new monodimensional azido-bridged manganese(II) complexes with empirical formulae $[Mn(N_3)_2(aminopyz)_2]_n$ (**1**), $[Mn(N_3)_2(4\text{-}azpy)_2]_n$ (**2**) and $[Mn(N_3)_2(4\text{-}Bzpy)_2]_n$ (**3**) (pyz = pyrazine (1,4-diazine)), 4-azpy = 4-azidopyridine and 4-Bzpy = 4-Benzoylpyridine), are reported. **1** is a monodimensional compound with double EO azido bridges, **2** is an alternating monodimensional compound with double end-on and double end-to-end azido bridges in the sequence di-EO-di-EE and **3** is a monodimensional compound with double end-on and double end-to-end azido bridges in the sequence di-EO-di-EO-diEO-di-EO-di-EE. The magnetic properties of **1-3** are reported. Periodic DFT calculations were performed to estimate the J values and Quantum Monte Carlo simulations were carried out using the calculated J values to check their accuracy in comparison with the experimental magnetic measurements. From this theoretical analysis, two appealing features of

[1] Electronic supplementary information (ESI) available: CCDC 1411985 (**1**) 1411986 (**2**) 1411987 (**3**). Table S1. For ESI and crystallographic data in CIF or other electronic format see DOI: …

the di-EO Mn(II) compounds can be extracted, first, the exchange coupling becomes more ferromagnetic when the Mn-N-Mn bridging angle becomes larger and the spin density of the bridging nitrogen atoms has an opposite sign than that of the Mn(II) centers.

Introduction

In the last years a plethora of polynuclear Mn(II)-azido bridging compounds have been prepared with the aim to expand the borders of the molecular magnetism field. One of the usual synthetic strategies mix the S = 5/2 Mn(II) cation with the potentially bridging azido ligand and a terminal L ligand to obtain a great number of compound with general formula $[Mn(N_3)_2(L)_2]$. L are usually R-pyridine monodentate ligands or $(L)_2$ one bidentate aromatic N-donor ligand. These $[Mn(N_3)_2(L)_2]$ compounds show all the range of dimensionalities: from molecular to 3D systems[1-13] Furthermore, the azido bridging ligand can show several coordination modes as the $\mu_{1,3}$ (end-to-end, EE) or $\mu_{1,1}$(end-on, EO) modes, which can be present simultaneously in the same compound, generating a great variety of topologies in 1D-3D compounds. Taking into account that the EE coordination mode typically promotes antiferromagnetic, AF, interactions and the EO coordination mode promotes ferromagnetic, F, interactions, the great diversity of dimensionalities and topologies found in the Mn(II)-azido bridging compounds has a consequence a great diversity in their magnetic behaviour: by example, in the 1D compound with bulk formula $[Mn(N_3)_2(3\text{-Mepy})_2]_n$ (3-Mepy = 3-methylpyridine) the sequence of the azido bridges is $(EE\text{-}EE\text{-}EO)_n$ which implies a $(AF\text{-}AF\text{-}F)_n$ interaction pattern and a ferrimagnetic behaviour in a homometallic chain.[14] This topological ferrimagnetism is found also in the 2D compound $[Mn(4\text{-}N_3py)_2(N_3)_2]_n$ (4-N_3py = 4-azidopyridine) with the same (EE-EE-EO) alternance pattern in two dimensions.[15a] As a consequence of their rich magnetic and structural variety, the polynuclear Mn(II)-azido bridging compounds have been also extensively used in magneto–structural correlations and theoretical studies.[1] We present in this work three monodimensional compounds which are new good examples of the wide structural and magnetic diversity found in the $[Mn(N_3)_2(L)_2]$ compounds: $[Mn(N_3)_2(aminopyz)_2]_n$ (**1**), $[Mn(N_3)_2(4\text{-}azpy)_2]_n$ (**2**) and $[Mn(N_3)_2(4\text{-}Bzpy)_2]_n$ (**3**) (pyz = pyrazine (1,4-diazine)), 4-azpy = 4-azidopyridine and 4-Bzpy = 4-Benzoylpyridine). **1** is a monodimensional compound with double EO azido bridges, **2** is a alternating monodimensional compound with double end-on and double

end-to-end azido bridges in the sequence di-EO-di-EE and **3** is a monodimensional compound with double end-on and double end-to-end azido bridges in the sequence di-EO-di-EO-diEO-di-EO-di-EE. A preliminary crystal structure of **2** was published recently.[15b] The magnetic properties of **1-3** are reported. The plot of $\chi_M T$ *vs* T for **1** can be fitted as homogeneous 1D system with J = 1.4(1) cm^{-1} and the plot of $\chi_M T$ *vs* T for **2** can be fitted as alternating F-AF 1D system with J_1 = -12.8(1) cm^{-1}, J_2 = 0.7(1) cm^{-1}. The exchange coupling constants J have been also calculated for **1-3** by using periodic DFT calculations. In order to check the accuracy of the calculated J values, Quantum Monte Carlo (QMC) simulations were performed to extract susceptibility curves that can be compared with the experimental ones. In general, such theoretical approach combining periodic calculations and QMC simulations is an accurate procedure to study the exchange interactions in extended structures due to the limitations of the fitting procedures of the experimental data.

Experimental Section

Starting Materials. Manganese(II) salts, organic N-donor ligands and sodium azide (Aldrich) were used as obtained. Aqueous hydrazoic acid is obtained with a modified Kipp's generator by decomposition of NaN_3 in H_2SO_4/H_2O (1:3, v:v) and subsequent transfer of HN_3 into H_2O with aid of an inert gas stream.[16] The use of diluted hydrazoic acid allows formation of an acidic medium with pH value < 5.5 without introducing a foreign salt, thus avoiding impurities. The synthesis of 4-azidopyridine was performed according to literature[17]

Caution! *Azide compounds and hydrazoic acid (HN_3) are potentially explosive! Only a small amount of material should be prepared and it should be handled with care.*

Spectral and Magnetic Measurements.

Infrared spectra (4000-400 cm^{-1}) were recorded from KBr pellets on a Perkin-Elmer 380-B spectrophotometer. Magnetic susceptibility measurements under several magnetic fields in the temperature range 2-300 K and magnetization measurements in the field range of 0-5 T were performed with a Quantum Design MPMS-XL SQUID magnetometer at the Magnetic Measurements Unit of the University of Barcelona. All measurements were performed on polycrystalline samples. Pascal's constants were used to estimate the diamagnetic corrections,

which were subtracted from the experimental susceptibilities to give the corrected molar magnetic susceptibilities.

Synthesis

$[Mn(N_3)_2(ampyz)_2]_n$ (**1**). Manganese(II) nitrate tetrahydrate (0.50 g, 2.0 mmol), sodium azide (0.26 g, 4.0 mmol) and aminopyrazine (0.19 g, 2.0 mmol) were dissolved in 3.5 mL aqueous hydrazoic acid. A clear solution was obtained after warming to 60°C. Slow cooling of the solution to 4°C gave after several days compound **1** as yellow crystals. Yield: 70%. Anal.: Found: C 29.0; H 3.0; N 51.3%. Calcd. for $C_8H_{10}MnN_{12}$: C 29.2; H 3.1; N 51.1%.

$[Mn(N_3)_2(4\text{-}azpy)_2]_n$ (**2**). Manganese(II) chloride dihydrate (0.161 g, 1.0 mmol) and 4-azidopyridine (0.240g, 2.0 mmol) were added to 10.0 mL dist. H_2O. NaN_3 aqueous solution (1M, 5mL) was then slowly added with stirring. The solution was then put into a compartment dryer (50° C) for four days. Afterwards the solution was stored at room temperature. Yellow crystals of **2** were obtained after some days. Yield: 84 %. Anal.: Found: C 31.7; H 2.4; N 51.5%. Calcd. for $C_{10}H_8MnN_{14}$: C 31.7; H 2.1; N 51.7%.

$[Mn(N_3)_2(4\text{-}Bzpy)_2]_n$ (**3**). To an aqueous solution (4 mL) of manganese(II) nitrate tetrahydrate (0.50 g, 2.0 mmol) and sodium azide (0.26 g, 4.0 mmol) 20 mL of methanolic solution of 4-Benzoylpyridine (0.37 g, 2.0 mmol) were added. The mixture was warmed to 60°C to obtain a clear solution and subsequently allowed to stand in an open beaker at room temperature. After two weeks yellow needle-shaped crystals of compound **3** were separated. Yield: 60%. Anal.: Found: C 56.9; H 3.5; N 22.4%. Calcd. for $C_{24}H_{18}MnN_8O_2$: C 57.0; H 3.6; N 22.2%.

IR spectra. In addition to the vibrations of the aromatic N-donor ligands, very strong absorption bands corresponding to the ν_{as} of the azido ligands appeared at 2100 cm^{-1} for **1**, at 2093 and 2054 cm^{-1} for **2**, and at 2105 and 2059 cm^{-1} for **3**, respectively.

X-ray Crystallography. The X-Ray single-crystal data of compounds **1-3** were collected on a Bruker SMART APEX CCD diffractometer with graphite-monochromated Mo Kα radiation (λ = 0.71073 Å). The crystallographic data, conditions retained for the intensity data collection and some features of the structure refinements are listed in Table 1. Data processing, Lorentz-polarization and absorption corrections were performed using SMART, APEX, SAINT, and SADABS[18], computer programs. The structures were solved by direct methods and refined by

full-matrix least-squares methods, using the SHELXTL program package.[19] All non-hydrogen atoms were refined anisotropically. The hydrogen atoms were located from difference Fourier maps, assigned with isotropic displacement parameters and included in the refinements by use of HFIX (parent C atoms) or DFIX (parent N atoms) utilities of the SHELXTL program package. Molecular plots were performed with the Mercury[20] program.

Please insert Table 1 close to here

Computational Methods. The computer code employed for the all calculations is the program SIESTA[21-23] (Spanish Initiative for Electronic Simulations with Thousands of Atoms) that allows handling periodic systems as those reported in this study. We have employed the generalized-gradient functional proposed by Perdew, Burke and Erzernhof[24] using the DFT+U option[25] with a U value of 4.0 eV. Only valence electrons are included in the calculations, with the core being replaced by norm-conserving scalar relativistic pseudopotentials factorized in the Kleinman-Bylander form.[26] The pseudopotentials are generated according to the procedure of Trouiller and Martins.[27] For the Mn atoms we have employed a pseudopotential including the 3s and 3p orbital in the basis set that we have previously tested to give accurate J values.[28] We also have employed a numerical basis set of triple-ζ quality with polarization functions for the manganese atoms and a double-ζ one with polarization functions for the main group elements. Previously, we have studied the influence of two main parameters of the SIESTA code, the energy shift and the mesh cut-off, in the calculated J value for transition metal systems.[29] Thus, the values of 50 meV for the energy shift and 250 Ry for mesh cut-off provide a good compromise between accuracy and computer time to estimate exchange coupling constants. The calculated J values are obtained with non-spin projected approach[30-33] and using the following Heisenberg-Dirac-van Vleck Hamiltonian:

$$\hat{H}^{HDVV} = -\sum_{i>j} J_{ij}\,\hat{S}_i\hat{S}_j \qquad (1)$$

A detailed description of how to calculate the J values of periodic systems was previously reported by some of us.[34] For the compound **1**, two calculations were performed to extract the unique J value as the energy difference between the high spin solution (both metal atoms in the unit cell with spin up) and the low spin solution (with the spin inversion of one the paramagnetic centers). For compounds **2** and **3**, three and six spin configurations were employed to calculate

the J values. A supercell duplicating the length in the direction of the chain must be create to calculate the exchange constants, thus, for compounds **1**, **2** and **3** in the periodic calculations the system has 62, 132 and 1060 atoms, respectively. Sets of 462, 12 and 1 k-points were employed, respectively for **1**, **2** and **3** to integrate the k-dependent properties.

The usual procedure to check the accuracy of the calculated J values is the generation of the χT curves for comparison with the experimental data. The best procedure for obtaining such curves is to perform exact diagonalization of the Hamiltonian. However, such approach cannot be applied for periodic systems and it is thus necessary to use approximate methods in order to perform a comparison with the experimental data. Quantum Monte Carlo methods represent a good alternative. Quantum Monte Carlo simulations based on the directed loop algorithm method developed by Sandvik et al.[35] were performed using the ALPS 2.0 library (dirloop_sse package).[36,37] For the susceptibility vs. temperature curve, usually we set 10^7 steps for simulations between 2 and 300 K and a whole simulation must be performed at each temperature. The initial 10% of steps was employed for thermalization of the system in all calculations. However, 10^9 steps were employed below in order to reach the convergence of the simulations using the DFT calculated J values.

Results and Discussion

Description of the structures

Description of the structure of $[Mn(N_3)_2(aminopyrazine)_2]_n$ (1)

Compound **1** crystallizes in the triclinic space group P-1. Relevant bond lengths and bond angles are listed in Table 2. Figure 1a illustrates the structure. Each Mn is coordinated by six N atoms in octahedral geometry. Four coordination sites are occupied by azido groups which double-bridge the Mn atoms in end-on only coordination mode to give 1-D chains along the a-axis of the unit cell [Mn..Mn = 3.4751(5) Å]. The octahedron is completed by two *trans* coordinated N atoms provided by two aminopyrazine ligands bonded via the aromatic nitrogen in meta position to the amino sidegroup. Mn(1) and the center of Mn(1)-N(11)-Mn(1b)-N(11b) rhomboid are located at centers of inversions. The azido group is out of the Mn_2N_2 plane with an angle of 159.5(2)° for N(11b)..N(11)-N(12). Both hydrogen atoms of the -NH_2 group establish hydrogen bonds to N

atoms in adjacent chains giving rise to a 2-D supramolecular network (Fig. 1b). Hydrogen acceptors are the terminal N atom of the azido groups and the non-coordinated aromatic N atom of the aminopyrazine ligands. Along the chain direction the pyrazine rings form π-π stacking interactions.

Please insert Table 2 and figures 1a and 1b close to here

Description of the structure of $[Mn(N_3)_2(4\text{-azpy})_2]_n$ (2).

The atom numbering scheme for complex **2** is given in Figure 2a, and selected bond parameters are collected in Table 3. The structure consists of octahedrally coordinated manganese atoms in which the coordination sites are occupied by two N atoms of the 4-azidopyridine ligands in *trans* arrangement and four azido ligands from double bridges between neighboring manganese atoms. The Mn-N bond lengths are in the range from 2.2156(11) to 2.2701(12) Å. The azido groups in the double bridges are alternatively in the EE and EO modes generating an alternating chain oriented along the *b*-axis of the triclinic unit cell (Fig.2b). The end-on azido bridges show asymmetric N-N distances of 1.2041(16)/1.1497(17) Å, whereas the end-to-end bridges are more symmetric: 1.1794(15)/1.1754(15) Å. The bond parameters within the $Mn_2(\mu_{1,3}\text{-}N_3)_2$ ring are: N(4)-Mn(1)-N(5) = 99.31(4)°, Mn(1)-N(5)-N(6) = 123.85(10)°, Mn(1)-N(4)-N(6b) = 119.91(9)°, torsion angle: Mn(1b)-N(5b)..N(4)-Mn(1) = 50.9°. This eight-membered ring $Mn_2(\mu_{1,3}\text{-}N_3)_2$ shows a distortion from the planar to a "chair"-like conformation with a δ-angle [defined as the dihedral angle between the plane defined for the six N-azido atoms and the N(4)-Mn(1)-N(5) plane] of 34.0°, whereas the four-membered $Mn_2(\mu_{1,1}\text{-}N_3)_2$ ring is planar. The intra-chain Mn..Mn distance within the four-membered ring is 3.6344(3) Å, and that within the eight-membered ring is 5.0301(3) Å, whereas the shortest interchain metal…metal separation is 8.2450(5) Å. The bond parameters of the di-EO azido bridge are: N(1)-Mn(1)-N(1a) = 81.25(5)°, Mn(1)-N(1a)-Mn(1a) = 98.75(5)°, Mn(1)-N(1)-N(2) = 126.07(9)°, Mn(1a)-N(1)-N(2) = 126.32(9)°, N(1a)..N(1)-N(2) "out-of plane angle" = 155.1(2)°. The azido ligands have N-N-N bond angles of 179.48(14)° and 178.74(14)°, respectively. The two axially bound 4-azidopyridine ligands show an angle of N(11)-Mn(1)-N(7) of 171.10(4)°. The reason for this deviation from 180° is due to the moving of the axial ligands away from the Mn_2N_2 ring. The covalent azido groups in para-position (from 4-azidopyridine) are highly asymmetric, with Δd(N-N) (difference of N-N bond lengths within the azide group) of 0.1355(18) Å and 0.1222(18) Å. The according bond angle for N(14)-N(13)-N(12) is 170.95(15)° and for N(10)-N(9)-N(8) is 171.14(15)°.

Please insert Table 3 and figures 2a and 2b close to here

Description of the structure of $[Mn(N_3)_2(4\text{-}Bzpy)_2]_n$ (3)

A perspective view of a section of the neutral polymeric $[Mn(4\text{-}Bzpy)_2(N_3)_2]_n$ chain of **3** together with the atom numbering scheme is given in Figure 3a, and selected bond parameters are collected in Table 4. The Mn(II) centers are octahedrally coordinated by two N donor atoms of the 4-Bzpy ligands in *trans*-arrangement and four N atoms of azido bridges. The Mn-N(N_3) bond distances are in the range from 2.221(4) to 2.248(4) Å, and the Mn-N(4-Bzpy) bond distances vary from 2.283(3) to 2.293(3) Å. The azido bridges show an alternating Mn(5)-$(EO)_2$-Mn(2)-$(EO)_2$-Mn(1)-$(EO)_2$-Mn(3)-$(EO)_2$-Mn(4)-$(EE)_2$- sequence giving rise to the 1D system, which is oriented along the *b*-axis of the monoclinic unit cell (Figure 3b). The Mn(4)-$(EE)_2$-Mn(5b) azido bridge has an almost planar arrangement with δ-angle of 3.6°. The Mn(4)..Mn(5b) intra-chain distance is 5.1413(13) Å, and the Mn(4)-N(51)..N(53b)-Mn(1b) torsion angle is -15.9°. The four-membered Mn_2N_2 rings formed by the four consecutive di-EO azido bridges have intra-chain metal..metal distances of 3.4693(12), 3.4735(12), 3.4634(12) and 3.4571(12) Å; and the Mn-N-Mn bond angles are in the range from 101.14(15) to 101.42(15)°. The angles N(X1a)..N(X1)-N(X2) (X = 1-4) are 175.0(4), 172.9(4), 176.1(4) and 174.1(4)°, respectively. The azido bridges have Mn-N-N and N-N-N bond angles varying from 123.6(3) to 135.3(3) and from 177.7(5) to 179.5(4)°, respectively. The trans-pyridine rings of the 4-Bzpy ligands are shifted towards the di-EE azido bridges [N(py)-Mn-N(py) bond angles: 178.24(18)° for Mn(1), 177.40(17)° for Mn(2), 174.02(16)° for Mn(3), 165.18(19)° for Mn(4) and 168.60(19)° for Mn(5), respectively]. Non-covalent ring-ring interactions are observed along the chain direction with separations of their centers of gravities in the range from 3.635 to 4.287 Å, for the pyridine rings and in the range from 3.770 to 3.870 Å, for the benzene rings of the 4-Bzpy ligands, respectively.

Please insert Table 4 and figures 3a and 3b close to here

Magnetic Data for$[Mn(N_3)_2(aminopyrazine)_2]_n$ (1)

The variable temperature magnetic susceptibility data for the title complex were recorded between 300 and 2 K. The plot of $\chi_M T$ *versus* T is shown in Figure 4. Compound **1** shows a $\chi_M T$ value of 4.85 $cm^3mol^{-1}K$ at room temperature, greater than the expected value for an isolated manganese atom (4.375 $cm^3mol^{-1}K$, g = 2.0), increases gradually as the temperature decreases to a maximum of 17.25 $cm^3mol^{-1}K$ at 5 K and then decreases quickly to 8.15 $cm^3mol^{-1}K$ at 2 K. The magnetic susceptibility behaviour of **1** indicates bulk ferromagnetic coupling in good agreement with magnetization

experiments which show a quasi-saturated value of M/Nβ equivalent to five electrons (5.13) under an external field of 5 T at 2K. Taking into account the 1D structure of **1**, the fit of the magnetic data was made by using the appropriate equation[38] for homogeneous S = 5/2 chains derived from the Hamiltonian $H = -JS_iS_{i+1}$ in the range 300-8 K due to the decrease of the $\chi_M T$ values after the maximum. The best fit parameters were J = 1.4(1) cm^{-1}, g = 2.09(1). The positive J value is in accordance with the ferromagnetic coupling expected for end-on azido bridges with Mn-N-Mn bond angles around 100º (the Mn(1)-N(11)-Mn(1') bond angle is 101.53(5)º). The found J value is similar to that reported for the related compounds *cis*-[Mn($\mu_{1,1}$-N_3)$_2$(2-bzpy)$_2$]$_n$ (2-bzpy = 2-benzoylpyridine)[39] and *trans*-[Mn($\mu_{1,1}$-N_3)$_2$(pyzamid)$_2$]$_n$ (pyzamid = pyrazineamide)[40] with J values of 0.8 and 1.1 cm^{-1} for Mn-N-Mn angles of 100.5º (mean angle) and 97.1º respectively. The structure of *cis*-[Mn($\mu_{1,1}$-N_3)$_2$(2-bzpy)$_2$]$_n$ shows well isolated chains but as in the case of *trans*-[Mn($\mu_{1,1}$-N_3)$_2$(pyzamid)$_2$]$_n$, **1** shows H bonds between chains which can be the cause of the weak antiferromagnetic interactions at low temperature as can be seen in the decrease of $\chi_M T$ in the low temperature region.

Please insert figure 4 close to here

Magnetic data for [Mn(N_3)$_2$(4-azpy)$_2$]$_n$ (2)

The variable temperature magnetic susceptibility data for the title complex were recorded between 300 and 2 K. The plot of χ_MT *versus* T is shown in Figure 5. Compound **2** shows a $\chi_M T$ value of 3.83 cm^{3}mol^{-1}K at room temperature, minor than the expected value for an isolated manganese atom (4.375 cm^{3}mol^{-1}K, g = 2.0), and decreases gradually as the temperature decreases to a minimum of 0.02 cm^{3}mol^{-1}K at 2 K. The magnetic susceptibility behaviour of **2** indicates bulk antiferromagnetic coupling in good agreement with magnetization experiments which show a quasi-saturated value of M/Nβ equivalent to zero electrons (0.06) under an external field of 5 T at 2K. Taking into account the alternating 1D structure of **2**, the fit of the magnetic data was made by using the appropriate equation[41] for ferromagnetic-antiferromagnetic coupled 1D S = 5/2 systems derived from the Hamiltonian $H = -J_1\Sigma S_{2i}S_{2i+1} - J_2\Sigma S_{2i+1}S_{2i+2}$. The best fit parameters were J_1 = -12.8(1) cm^{-1}, J_2 = 0.7(1) cm^{-1}, g = 2.06(1). The positive J value is in accordance with the ferromagnetic coupling expected for end-on azido bridges with Mn-N-Mn bond angles around 100º (the Mn(1)-N(1a)-Mn(1a) bond angle is 98.75(5)º). The found J value is similar to that reported for the related compounds *cis*-[Mn($\mu_{1,1}$-N_3)$_2$(2-bzpy)$_2$]$_n$ (2-bzpy = 2-benzoylpyridine)[39] and *trans*-[Mn($\mu_{1,1}$-

$N_3)_2(pyzamid)_2]_n$ (pyzamid = pyrazineamide)[40] with J values of 0.8 and 1.1 cm^{-1} for Mn-N-Mn angles of 100.5º (mean angle) and 97.1º respectively.

Please insert figure 5 close to here

Magnetic data for $[Mn(N_3)_2(4\text{-}Bzpy)_2]_n$ (3)

The plot of $\chi_M T$ *versus* T in the 300-2 K range of temperature for compound **3** is shown in Figure 6. Compound **3** shows a $\chi_M T$ value of 4.31 $cm^3mol^{-1}K$ at room temperature, similar than the expected value for an isolated manganese atom (4.375 $cm^3mol^{-1}K$, g = 2.0). On cooling, $\chi_M T$ decreases to 3.72 $cm^3mol^{-1}K$ at 60 K. Below this broad minimum, $\chi_M T$ increases to a maximum of 3.87 $cm^3mol^{-1}K$ at 20 K and then falls to 1.18 $cm^3mol^{-1}K$ at 2 K. The magnetization measurements show a saturation value close to S = 3/2 per manganese ion (Inset of Figure 6). This value is striking as the ground state of this chain should be S = 0 (Scheme 1). The $\chi_M T$ decay observed below 20 K corresponds to the population of the ground state. Similar behaviour has been observed in the 1D compound[14] *trans*-$[Mn(N_3)_2(Menic)_2]_n$ showing the same topology than **3.**

Please insert figures 6 and scheme 1 close to here

Theoretical Study

The structural dependence of the exchange coupling in end-on azido-bridged Mn(II) dinuclear complexes were previously study by using hybrid DFT methods.[42] Thus, it is expected that end-on coordination results in ferromagnetic behavior[43] while the opposite is found for end-to-end azido bridging ligands. The calculated values for the three studied systems are collected in Table 5. It is worth noting that generalized gradient approximation functionals, as PBE, are less accurate than hybrid functionals to calculate the J values.[30-33] However, computer codes to calculate periodic systems usually have not implemented hybrid functionals in an efficient way, hence, we have employed the PBE functional that usually gives good results for transition metal complexes. The calculated J values show that the PBE functional reproduce properly the sign of the interaction, thus, exchange coupling through end-on azido ligands are ferromagnetic while those with end-to-end coordination are stronger and antiferromagnetic. In order to perform a comparison with the experimental data, the calculated DFT J values (see Table 5) were employed joint with Quantum Monte Carlo simulations (see Computational details section) to calculate magnetic susceptibility curves that can be directly compare with the experimental data. An excellent agreement is found in

Figure 7 showing that the employed DFT methodology is able to reproduce the experimental magnetic properties of these systems.

Please insert Table 5 and figure 7 close to here

Concerning the strength of the interaction, there is a "general believe" that the increase of the M-X-M angle for bridging ligands with a single atom in the exchange pathway enhances the antiferromagnetic contributions. As mentioned above, previously we performed a theoretical study using B3LYP functional to analyze the dependence between J and the Mn-N-Mn bridging angle for dinuclear azido ligands, as well as for the equivalent systems with Cu(II) and Ni(II) cations. In the three cases, there is a parabolic dependence showing a maximum of the parabola that corresponds to the strongest ferromagnetic coupling.[42] This maximum appears at M-N-M angle values of 85º, 102º and 112º for Cu(II), Ni(II) and Mn(II) complexes, respectively. Thus, as most of the Cu(II) complexes have an Cu-N-Cu angle larger than 85º the tendency is in agreement with the "expected" behavior, larger Cu-N-Cu increases the antiferromagnetic contribution and the complexes become less ferromagnetic. For the Ni(II) complexes, the maximum strength of the ferromagnetic interaction appears for Ni-N-Ni angle value close to those adopted in most of the structures.[44] Thus, most of Ni(II) azido bridging complexes show a small dispersion in the J values being ferromagnetic only a reported complex with a Ni-N-Ni angle value close to 90º presents antiferromagnetic behavior.[45] However, the Mn(II) complexes adopt Mn-N-Mn angle values smaller than that corresponding to the strongest ferromagnetic coupling. Thus, an increase of the Mn-N-Mn enhances the ferromagnetism and such tendency is just the opposite to the usually assumed. This fact can be corroborated in Figure 8 showing the dependence of the fitted J value for the reported EO azido Mn(II) complexes with the Mn-N-Mn angle value.

Please insert figure 8 close to here

The calculated spin density of the compound **1** is represented in Figure 9. Surprisingly, the spin density of the bridging nitrogen atom of the azido groups shows negative spin density (-0.07 e^-) despite that the d^5 configuration of the Mn(II) cations (spin population 4.8 e^-). Such electronic configuration implies the occupation of the "e_g" antibonding orbitals with a large mixing with the ligand orbitals, thus, it should be expected that such large orbital mixing will provide the same sign in the spin density of all the nitrogen atoms coordinated to the metal (spin delocalization mechanism) as happens with the pyrazine ligands (see Fig. 8).[61,62] However, the opposite sign in such atoms indicate (also appears in compounds **2** and **3**) that the spin polarization mechanism is predominant,

this result is different to that obtained either theoretically or experimentally for similar Cu(II) complexes.[42]

Please insert figure 9 close to here

In order to check if the opposite sign of the spin population of the bridging nitrogen atom is an artifact of the periodic PBE pseudopotential calculations, we performed all electron[63] calculations of one Mn(II) end-on diazido dinuclear complex (FIBJIK see Table S1)[48] with the hybrid B3LYP functional[64] using the Gaussian code.[65] Again, such results confirm the negative spin population of the bridging nitrogen atoms (-0.05 e^-). The sign of the spin density in such nitrogen atoms is a subtle interplay between the spin delocalization of the singly-occupied antibonding e_g-type orbitals and the spin polarization caused by the also singly-occupied t_{2g}-type orbitals. Usually, in such case with singly-occupied antibonding e_g-type orbitals the spin delocalization prevails over the spin polarization, as found in Fig. 9 for the pyrazine ligands. However, the azido ligand has two π frontier orbital (HOMO and LUMO) that very weakly interact with the in-phase and out-of-phase combination of the two d_{x2-y2} metal orbitals.[66] Thus, the two resulting molecular orbitals remain almost degenerate being consistent with the ferromagnetic character of the complexes with end-on azido bridging ligands. The weak interaction between the metal-azido orbitals results in a poor spin delocalization contribution (also reflected in high spin population value of the Mn(II) centers around 4.8 e^-) that is overcome by the spin polarization. To corroborate such assumptions, we repeated the DFT calculations for the dinuclear complex replacing the Mn(II) by Ni(II) cations (unpaired electrons in the two e_g-type orbitals, only spin delocalization) and V^{II} cations (unpaired electrons in the three t_{2g}-type orbitals, only spin polarization). In the case of the hypothetical dinuclear Ni(II) complex the spin population in the bridging nitrogen atom is only +0.02e^- while in the equivalent V^{II} system the value is -0.07 e^- showing the predominance of the spin polarization. Finally, it is worth to point out that the spin distribution found in the Mn(II) end-on diazido dinuclear complexes is similar to that proposed by Kahn and coworkers for Cu(II) end-on diazido dinuclear systems based on the so-called "spin polarization mechanism" [67] with opposite spin population in the bridging nitrogen atom while the terminal azido nitrogen atom has a relatively larger spin population with the same sign than the metal centers (see Fig. 8). This spin distribution was ruled out, either experimentally[68] or theoretically[42] for dinuclear Cu(II) systems but now we found that is present in the Mn(II) systems.

Despite this fact the presence of ferromagnetic coupling in the family of end-on diazido dinuclear complexes is due to the accidental orthogonality of the orbitals bearing the unpaired electrons. [69]

Conclusions

Here we have presented three new compounds with azido as bridging ligand synthesized from the S = 5/2 Mn(II) cation and a terminal L ligand. The new compounds are: $[Mn(N_3)_2(aminopyz)_2]_n$ (**1**), $[Mn(N_3)_2(4\text{-azpy})_2]_n$ (**2**) and $[Mn(N_3)_2(4\text{-Bzpy})_2]_n$ (**3**) (pyz = pyrazine (1,4-diazine)), 4-azpy = 4-azidopyridine and 4-Bzpy = 4-Benzoylpyridine),. The general formula is $[Mn(N_3)_2(L)_2]$, The compounds **1-3** are representative of the the great diversity of dimensionalities and topologies found in the Mn(II)-azido bridging compounds: **1** is a monodimensional compound with double EO azido bridges, **2** is a alternating monodimensional compound with double end-on and double end-to-end azido bridges in the sequence di-EO-di-EE and **3** is a monodimensional compound with double end-on and double end-to-end azido bridges in the sequence di-EO-di-EO-diEO-di-EO-di-EE. Periodic calculations using PBE functionals to calculate the J values provide an excellent agreement with the experimental data. The comparison was performed by using Quantum Monte Carlo simulations that allow to calculate magnetic susceptibility curves for periodic systems. Also, it is work noting that the theoretical analysis allows to propose that in the range of the experimental Mn-N-Mn bridging angle values, the calculated and observed trend is that larger angles results in stronger ferromagnetic coupling. Such tendency is just the opposite one to that usually expected, and found in Cu(II) and Ni(II) complexes. The DFT spin density of the bridging nitrogen atoms of the azido ligands has the opposite sign of that of the Mn(II) centers. This result is not common because usually in the cases that the metals centers have unpaired electrons in the antibonding orbitals, the large metal-ligand mixing of orbitals results in that the spin delocalization effects are predominant over the spin polarization. In the studied end-on azido Mn(II) systems, the weak metal-ligand interaction is reflected in that the resulting molecular orbitals are close to the degeneracy, and that the spin polarization effects induced by the three singly-occupied "non-bonding" t_{2g}-type orbitals of the Mn(II) centers overcome the delocalization effect of the e_g-type orbitals. Logically, such "special" behavior cannot be found in Cu(II) or NI(II) equivalent complexes because the t_{2g}-type orbitals are doubly-occupied.

Acknowledgments. R. V. acknowledge the financial support from Spanish government grant CTQ2012-30662 and the Generalitat de Catalunya (Grant 2009SGR1454). E. R. acknowledges for an ICREA Academia grant (Generalitat de Catalunya) and for the grant CTQ2011-23862-C02-01 to the Spanish government. L. M. thanks *Conicyt-Chile* for a pre-doctoral fellowship. Computer resources, technical expertise and assistance provided by the Barcelona Supercomputing Centre.

Supporting Information Available: Table S1. Reported Mn(II) end-on azido compounds (labeled with the CSD REFCODE) showing the Mn-N-Mn bond angles (in degrees) and the experimental exchange coupling constants J (cm^{-1}) for such compounds.

Legends for Scheme 1 and Figures:

Scheme 1: Ground state for an $(AF\text{-}F\text{-}F\text{-}F\text{-}F\text{-})_n$ interaction sequence.

Figure 1. (a) Perspective view of **1** showing the atom-numbering scheme. Symmetry codes: (a) -x+1,-y+1,-z; (b) -x+2,-y+1,-z; (c) x-1,y,z. (b) Packing view of **1**. Broken bonds indicate hydrogen bonds.

Figure 2. (a) A section of the chain structure of **2** showing the atom-numbering scheme. Symmetry codes: (a) -x+2,-y,-z; (b) -x+1,-y,-z; (c) x+1,y,z. (b) Packing view of **2**.

Figure 3. (a) A section of the 1-D system of **3** showing the atom-numbering scheme. Symmetry codes: (a) -x,y,1/2-z; (b) x,1+y,z; (c) x,-1+y,z ; (d) –x,1+y,1/2-z; (e) –x,-1+y,1/2-z. (b) Packing view of **3**

Figure 4. $\chi_M T$ *vs* T plot in the 300-2 K range of temperatures for **1**. The solid line shows the best fit as uniform chain (see text).

Figure 5. $\chi_M T$ *vs* T plot in the 300-2 K range of temperatures for **2**. The solid line shows the best fit as alternating chain (see text).

Figure 6. $\chi_M T$ *vs* T plot in the 300-2 K range of temperatures for **3**. **Inset:** Molar magnetization at 2 K for (**3**).

Figure 7. $\chi_M T$ *vs* T plot in the 300-2 K range of temperatures for **1** (squares), **2** (triangles) and **3** (circles). The $\chi_M T$ **v**alues obtained by means of Quantum Monte Carlo simulations using the calculated DFT J values are plotted as continuous lines.

Figure 8. Representation of the dependence of the reported experimental J values for dinuclear (black circles)[43,46-54] and chain (black squares)[10,55-60] azido-bridged Mn(II) compounds and those calculated in this work (white circles).

Figure 9. Calculated spin density of the compound **1**. White and blue isodensity surfaces indicate positive and negative spin populations, respectively with a value of 0.003 $e^-/bohr^3$.

Table 1. Crystal Data and Structure Refinement for Complexes **1-3**

Compound	**1**	**2**	**3**
Empirical formula	$C_8H_{10}MnN_{12}$	$C_{10}H_8MnN_{14}$	$C_{120}H_{90}Mn_5N_{40}O_{10}$
Formula weight	329.22	379.24	2527.03
Crystal system	Triclinic	Triclinic	Monoclinic
Space group	P-1	P-1	C 2/c
a (Å)	3.4751(5)	8.2450(3)	37.0077(13)
b (Å)	7.7427(7)	8.3050(3)	19.0045(7)
c (Å)	12.4280(14)	11.9444(5)	17.0615(6)
α (°)	101.48(2)	82.612(2)	90
β (°)	96.04(2)	69.905(2)	112.212(2)
γ (°)	96.73(2)	80.754(2)	90
V (Å^3)	322.60(7)	755.74(5)	11109.1(7)
Z	1	2	4
T (K)	100(2)	100(2)	100(2)
ρ_{calcd} (g m^{-3})	1.695	1.667	1.511
μ (mm^{-1})	1.040	0.904	0.635
Crystal size (mm)	0.35×0.18×0.08	0.38×0.22×0.17	0.48×0.14×0.11
θ_{max} (°)	26.35	31.70	25.30
Reflections collected	2589	23052	62737
R(int)	0.0219	0.0274	0.0523
Data	1298	4813	10123
Parameters	107	226	791
R^a [$I > 2\sigma(I)$]	0.0452	0.0291	0.0455
$R^2\omega^b$ (all data)	0.1107	0.0688	0.1656

[a]$R(F_o) = \Sigma \| F_o | - | F_c \| / \Sigma | F_o |$; [b]$R\omega(F_o)^2 = \{\Sigma[\omega((F_o)^2-(F_c)^2)^2]/\Sigma[\omega((F_o)^4]\}^{1/2}$

Table 2. Selected bond lengths (Å) and angles (°) for (**1**).

Mn(1)...Mn(1b)	3.4751(5)	Mn(1)-N(11a)	2.232(2)
Mn(1)-N(11c)	2.250(2)	Mn(1)-N(1a)	2.272(2)
N(11)-N(12)	1.212(3)	N(12)-N(13)	1.148(3)
N(3)-H(5)	0.79	H(5)...N(13d)	2.36
N(3)...N(13d)	3.121(4)	N(3)-H(6)	0.84
H(6)...N(2e)	2.20	N(3)...N(2e)	3.037(3)
N(11a)-Mn(1)-N(11)	180.0	N(11a)-Mn(1)-N(11b)	101.53(5)
N(11)-Mn(1)-N(11b)	78.47(5)	N(11b)-Mn(1)-N(11c)	180.0
N(11a)-Mn(1)-N(1a)	91.07(9)	N(11c)-Mn(1)-N(1a)	92.58(9)
N(11b)-Mn(1)-N(1a)	87.42(9)	N(11a)-Mn(1)-N(1)	88.93(9)
N(1a)-Mn(1)-N(1)	180.0	N(12)-N(11)-Mn(1)	132.26(19)
N(12)-N(11)-Mn(1b)	120.74(19)	Mn(1)-N(11)-Mn(1b)	101.67(9)
N(13)-N(12)-N(11)	179.4(3)	N(11b)..N(11)-N(12)	159.5(2)
N(3)-H(5)...N(13d)	162	N(3)-H(6)...N(2e)	174

Symmetry codes: (a) -x+1,-y+1,-z; (b) -x+2,-y+1,-z; (c) x-1,y,z; (d) x-1,y+1,z; (e) -x+1,-y+2,-z+1

Table 3. Selected bond lengths (Å) and angles (°) for (**2**).

Mn(1a)-N(1)	2.2156(11)	Mn(1)-N(1)	2.2172(11)
Mn(1)-N(11)	2.2369(12)	Mn(1)-N(4)	2.2400(12)
Mn(1)-N(5)	2.2450(12)	Mn(1)-N(7)	2.2701(12)
N(1)-N(2)	1.2041(16)	N(2)-N(3)	1.1497(17)
N(5)-N(6)	1.1754(15)	N(6)-N(4b)	1.1794(15)
N(4b)-N(6)	1.1795(15)	N(11)-C(6)	1.3384(18)
N(11)-C(10)	1.3403(18)	N(12)-N(13)	1.2536(17)
N(12)-C(8)	1.4113(18)	N(13)-N(14)	1.1181(17)
N(7)-C(5)	1.3379(18)	N(7)-C(1)	1.3411(17)
N(8)-N(9)	1.2465(17)	N(8)-C(3)	1.4139(18)
N(9)-N(10)	1.1243(17)		
N(1a)-Mn(1)-N(1)	81.25(5)	N(1a)-Mn(1)-N(11)	94.13(4)
N(1)-Mn(1)-N(11)	93.82(4)	N(1a)-Mn(1)-N(4)	170.27(4)
N(1)-Mn(1)-N(4)	89.33(4)	N(11)-Mn(1)-N(4)	88.93(4)
N(1a)-Mn(1)-N(5)	90.09(4)	N(1)-Mn(1)-N(5)	171.34(4)
N(11)-Mn(1)-N(5)	86.79(4)	N(4)-Mn(1)-N(5)	99.31(4)
N(1a)-Mn(1)-N(7)	91.85(4)	N(1)-Mn(1)-N(7)	93.60(4)
N(11)-Mn(1)-N(7)	171.10(4)	N(4)-Mn(1)-N(7)	86.25(4)
N(5)-Mn(1)-N(7)	86.62(4)	N(2)-N(1)-Mn(1a)	126.32(9)
N(2)-N(1)-Mn(1)	126.07(9)	Mn(1a)-N(1)-Mn(1)	98.75(5)
N(3)-N(2)-N(1)	179.48(14)	N(6)-N(5)-Mn(1)	123.85(10)
N(5)-N(6)-N(4b)	178.74(14)	N(6)-N(4)-Mn(1b)	119.91(9)
C(6)-N(11)-C(10)	116.87(12)	C(6)-N(11)-Mn(1)	120.85(9)
C(10)-N(11)-Mn(1)	122.28(10)	N(13)-N(12)-C(8)	116.50(12)
N(14)-N(13)-N(12)	170.95(15)		

Symmetry codes: (a) –x,1-y,1-z; (b) –x,-y,1-z.

Table 4. Selected bond lengths (Å) and angles (°) for (**3**).

Mn(1)-N(11)	2.243(4)	Mn(2)-N(11)	2.240(4)
Mn(1)-N(31)	2.248(4)	Mn(2)-N(21)	2.240(4)
Mn(1)-N(1)	2.289(3)	Mn(2)-N(2)	2.293(3)
Mn(3)-N(31)	2.242(4)	Mn(4)-N(41)	2.239(4)
Mn(3)-N(41)	2.236(4)	Mn(4)-N(51)	2.221(4)
Mn(3)-N(3)	2.291(3)	Mn(4)-N(4)	2.283(3)
Mn(5)-N(21)	2.236(4)	N(11)-N(12)	1.186(5)
Mn(5)-N(53)	2.221(4)	N(12)-N(13)	1.152(5)
Mn(5)-N(5)	2.287(4)	N(21)-N(22)	1.178(5)
N(22)-N(23)	1.156(6)	N(31)-N(32)	1.181(5)
N(32)-N(33)	1.153(6)	N(41)-N(42)	1.192(5)
N(42)-N(43)	1.144(6)	N(51)-N(52)	1.160(5)
N(52)-N(53b)	1.176(5)		
N(11)-Mn(1)-N(31)	179.34(13)	N(1)-Mn(1)-N(1a)	178.24(18)
N(11)-Mn(2)-N(21a)	179.74(12)	N(2)-Mn(2)-N(2a)	177.40(17)
N(41a)-Mn(3)-N(31)	178.65(13)	N(3)-Mn(3)-N(3a)	174.02(16)
N(41)-Mn(4)-N(51a)	168.48(15)	N(4)-Mn(4)-N(4a)	165.18(19)
N(21)-Mn(5)-N(53)	168.76(15)	N(5)-Mn(5)-N(5a)	168.60(19)
Mn(1)-N(11)-N(12)	130.4(3)	Mn(2)-N(11)-N(12)	127.8(3)
Mn(2)-N(21)-N(22)	134.4(3)	Mn(5)-N(21)-N(22)	123.9(3)
Mn(1)-N(31)-N(32)	130.7(3)	Mn(3)-N(31)-N(32)	127.7(3)
Mn(3)-N(41)-N(42)	135.3(3)	Mn(4)-N(41)-N(42)	123.6(3)
Mn(4)-N(51)-N(52)	127.4(3)	Mn(5)-N(53)-N(52c)	127.9(3)
Mn(1)-N(11)-Mn(2)	101.42(15)	Mn(2)-N(21)-Mn(5)	101.37(15)
Mn(1)-N(31)-Mn(3)	101.35(15)	Mn(3)-N(41)-Mn(4)	101.14(15)
N(11)-N(12)-N(13)	179.5(4)	N(21)-N(22)-N(23)	179.4(5)
N(31)-N(32)-N(33)	179.2(4)	N(41)-N(42)-N(43)	179.2(4)
N(51)-N(52)-N(53b)	177.7(5)		

Symmetry codes: (a) –x,y,1/2-z; (b) x,1+y,z; (c) x,-1+y,z; (d) –x,1+y,1/2-z; (e) –x,-1+y,1/2-z.

Table 5. Description of the bridging ligands, Mn···Mn and Mn-X distances (in Å) and bond angles (in degrees), and calculated exchange coupling constants J (cm^{-1}) for the compounds **1**-**3**. The calculated values were obtained using the PBE functional with the SIESTA code (see Computational details section) and J_{fit} values are those extracted from the experimental measurements using a ring model.

	Bridging ligands	Mn···Mn	Mn-N	Mn-N-Mn	J_{PBE}	J_{fit}
1						
J_1	two EO μ_2-N_3	3.475	2.250-2.232-2.250-2.232	101.65	+2.4	+1.4
2						
J_1	two EO μ_2-N_3	3.364	2.217-2.216-2.217-2.216	98.75	+0.12	+0.7
J_2	two EE μ_2-N_3	5.030	2.240-2.245-2.245-2.240		-10.4	-12.8
3						
J_1	two EO μ_2-N_3	3.474	2.248-2.248-2.242-2.242	101.38	+1.6	
J_2	two EO μ_2-N_3	3.457	2.235-2.235-2.240-2.240	101.15	+1.6	
J_3	two EO μ_2-N_3	5.141	2.239-2.239-2.243-2.243	101.39	+1.5	
J_4	two EO μ_2-N_3	3.465	2.237-2.237-2.241-2.241	101.37	+1.3	
J_5	two EE μ_2-N_3	5.141	2.221-2.221-2.220-2.220		-14.6	

References

(1) J. Ribas, A. Escuer, M. Monfort, R. Vicente, R. Cortés, L. Lezama and T. Rojo, *Coord. Chem. Rev.* 1999, **193-195**, 1027.

(2) B. Bitschnau, A. Egger, A. Escuer, F.A. Mautner, B. Sodin, and R. Vicente, *Inorg. Chem.* 2006, **45**, 868. *and references therein.*

(3) X.-Y. Wang, B.-L. Li, X. Zhu, and S. Gao, *Eur. J. Inorg. Chem.* 2005, 3277.

(4) M.A.M. Abu-Youssef, A. Escuer, and V. Langer, *Eur. J. Inorg. Chem.* 2005, 4659.

(5) W. Zhao, Y. Song, T.-A. Okamura, J. Fan, W.-Y. Sun, and N. Ueyama, *Inorg. Chem.* 2005, **44**, 3330.

(6) E.-Q. Gao, A.-L. Cheng, Y.-X. Xu, M.-Y. He, and C.-H. Yan, *Inorg. Chem.* 2005, **44**, 8822.

(7) H.-R. Wen, C.-F. Wang, Y. Song, J.-L. Zuo, and X.-Z. You, *Inorg. Chem.* 2005, **44**, 9039.

(8) M. A. M. Abu-Youssef, A. Escuer, and V. Langer, *Eur. J. Inorg. Chem.* 2006, 3177.

(9) S.Q. Bai, E. Q. Gao, Z. He, C.-J. Fang, Y.-F. Yue, and C.-H. Yan, *Eur. J. Inorg. Chem.* 2006, 407.

(10) A. Das, G. M. Rosair, M. Salah El Fallah, J. Ribas, and S. Mitra, *Inorg. Chem.* 2006, **45**, 3301.

(11) P. Bhuina, V. S. Ray, G. Mostafa, J. Ribas, and C. Sinha, *Inorg. Chim. Acta.* 2006, **359**, 4660.

(12) F.-C. Liu, Y.-F. Zeng, J.-P. Zhao, B.-W. Hu, X.-H. Bu, J. Ribas, and J. Cano, *Inorg. Chem.* 2007, **46**, 1520.

(13) J.-Y. Zhang, C.-M. Liu, D.-Q. Zhang, S. Gao, and D.-B. Zhu, *Inorg. Chem. Commun.*, 2007, **10**, 897.

(14) M.A.M. Abu-Youssef, A. Escuer, M. A. S. Goher, F. A. Mautner, G. J. Reiss, R. Vicente *Angew. Chem., Int. Ed.* 2000, 39, 1624.

(15) (a) A. Escuer, F. A. Mautner, M. A. S. Goher, M.A.M. Abu-Youssef, R. Vicente, *Chem. Commun*., 2005, 605; (b) F.A. Mautner, A. Egger, B. Sodin, M.A.S. Goher, M.A.M. Abu-Youssef, A. Massoud, A. Escuer, R. Vicente, *J. Mol. Struct*. 2010, **969**, 192.

(16) (a) T.A. Richter, Energetic Materials, ed. H.D. Fair and R.F. Walker, Plenum Press, New York, 1977, vol I, pp. 25-31; (b) R. Vicente, B. Bitschnau, A. Egger, B. Sodin, F.A. Mautner, *Dalton Trans.*, 2009, 5120.

(17) G. Labbe, L. Beenaerts, *Tetrahedron*, 1989, **45**, 749.

(18) SADABS Bruker AXS, Software Reference Manual, Madison, WI, 1998.

(19) G.M. Sheldrick, *Acta Crystallogr., Sect. A: Found. Crystallogr.*, 2008, **64**, 112.

(20) C.F. Macrae, P.R. Edington, P. McCabe, E. Pidcock, G.P. Shields, R. Taylor, T. Towler, J. van de Streek, *J. Appl. Crystallogr.* 2006, **39**, 453.

(21) *Siesta 3.0*: E. Artacho, J.M. Cela, J.D. Gale, A. García, J. Junquera, R.M. Martin, P. Ordejón, D. Sánchez-Portal, J.M. Soler, 2010.

(22) E. Artacho, D. Sánchez-Portal, P. Ordejón, A. García, J.M. Soler, *Phys. Stat. Sol. A* 1999, **215**, 809..

(23) J.M. Soler, E. Artacho, J.D. Gale, A. García, J. Junquera, P. Ordejón, D. Sánchez-Portal, *J. Phys.: Condens. Matter* 2002, **14**, 2745.

(24) J. Perdew, K. Burke, M. Ernzerhof, *Phys. Rev. Lett.* 1996, **77**, 3865.

(25) V.I. Anisimov, F. Aryasetiawan, A.I. Lichtenstein, J. Phys.: Condens. Matter, 1997, **9**, 767.

(26) L. Kleinman, D.M. Bylander, *Phys. Rev. Lett.* 1982, **48**, 1425.

(27) N. Trouiller, J.L. Martins, *Phys. Rev. B* 1991, **43**, 1993.

(28) E. Ruiz, T. Cauchy, J. Cano, R. Costa, J. Tercero, S. Alvarez, *J. Am. Chem. Soc.* 2008, **130**, 7420.

(29) E. Ruiz, A. Rodríguez-Fortea, J. Tercero, T. Cauchy, C. Massobrio, *J. Chem. Phys.* 2005, **123**, 074102.

(30) E. Ruiz, P. Alemany, S. Alvarez, J. Cano, *J. Am. Chem. Soc.* 1997, **119**, 1297.

(31) E. Ruiz, S. Alvarez, J. Cano, V. Polo, *J. Chem. Phys.* 2005, **123**, 164110.

(32) E. Ruiz, *Struct. Bond.* 2004, **113**, 71.

(33) E. Ruiz, A. Rodríguez-Fortea, J. Cano, S. Alvarez, P. Alemany, *J. Comp. Chem.* 2003, **24**, 982.

(34) E. Ruiz, M. Llunell, P. Alemany, *J. Solid State Chem.* 2003, **176**, 400.

(35) A.W. Sandvik, *Phys. Rev. B* 1999, **59**, 14157.

(36) A.F. Albuquerque, F. Alet, P. Corboz, P. Dayal, A. Feiguin, S. Fuchs, L. Gamper, E. Gull, S. Gürtler, A. Honecker, R. Igarashi, M. Körner, A. Kozhevnikov, A. Läuchli,

S.R. Manmana, M. Matsumoto, I.P. McCulloch, F. Michel, R.M. Noack, G. Pawlowski, L. Pollet, T. Pruschke, U. Schollwöck, S. Todo, S. Trebst, M. Troyer, P. Werner, S. Wessel, *J. Magn. Magn. Mat.* 2007, **310**, 1187.

(37) B. Bauer, L.D. Carr, H.G. Evertz, A. Feiguin, J. Freire, S. Fuchs, L. Gamper, J. Gukelberger, E. Gull, S. Guertler, A. Hehn, R. Igarashi, S.V. Isakov, D. Koop, P.N. Ma, P. Mates, H. Matsuo, O. Parcollet, G. Pawłowski, J.D. Picon, L. Pollet, E. Santos, V.W. Scarola, U. Schollwöck, C. Silva, B. Surer, S. Todo, S. Trebst, M. Troyer, M.L. Wall, P. Werner, S. Wessel, *J. Stat. Mech. Theor. Exp.* 2011, **2011**, P05001.

(38) M. E. Fisher, Am. J. Phys. 1964, **32** 343.

(39) M.A.M. Abu-Youssef, A. Escuer, D. Gatteschi, M. A. S. Goher, F. Mautner, R. Vicente, *Inorg. Chem.* 1999, **38**, 5716.

(40) M.A.M. Abu-Youssef, A. Escuer, V. Langer, *Eur. J. Inorg. Chem.* 2006, 3177.

(41) R. Cortés, M. Drillon, X. Solans, L. Lezama and T. Rojo, *Inorg. Chem.* 1997, **36**, 677.

(42) E. Ruiz, J. Cano, S. Alvarez, P. Alemany, *J. Am. Chem. Soc.* 1998, **120**, 11122.

(43) T.K. Karmakar, B.K. Ghosh, A. Usman, H.-K. Fun, E. Rivière, T. Mallah, G. Aromí, S.K. Chandra, *Inorg. Chem.* 2005, **44,** 2391.

(44) G. Manca, J. Cano, E. Ruiz, *Inorg. Chem.* 2009, **48**, 3139.

(45) P. Chaudhuri, R. Wagner, S. Khanra, T. Weyhermuller, *Dalton Trans.* 2006, 4962.

(46) H. Hosseini-Monfared; R. Bikas; J. Sanchiz, T. Lis, M. Siczek, J. Tucek, R.Zboril; P. Mayer, *Polyhedron* 2013, **61**, 45.

(47) H.-P. Jia, W. Li, Z.-F. Ju, J. Zhang, *Inorg. Chem. Commun.* 2007, **10**, 397.

(48) C.-M. Liu, S. Gao, D.-Q. Zhang, Z.-L. Liu, D.-B. Zhu, *Inorg. Chim. Acta* 2005, **358**, 834.

(49) R. Cortes; J.L. Pizarro; L. Lezama; M.I. Arriortua; T. Rojo, *Inorg.Chem.* 1994, **33**, 2697.

(50) H.-Y. Wu, H.-Q. An, B.-L. Zhu, S.-R. Wang, S.-M. Zhang, S.-H. Wu, W.-P. Huang, *Inorg. Chem. Commun*. 2007, **10**, 1132.

(51) M.-M. Yu, Z.-H. Ni, C.-C. Zhao, A.-L. Cui, H.-Z. Kou, *Eur. J. Inorg. Chem*. 2007, 5670.

(52) Z.-S. Meng, L. Yun, W.-X. Zhang, C.-G. Hong, R. Herchel; Y.-C. Ou, J.-D. Leng, M.-X. Peng, Z.-J. Lin, M.-L. Tong, *Dalton Trans*. 2009, 10284.

(53) Z.-H. Ni, H.-Z. Kou, L. Zheng, Y.-H. Zhao, L.-F. Zhang, R.-J. Wang, A.-L. Cui, O. Sato, *Inorg. Chem*. 2005, **44**, 4728.

(54) C.-H. Ge, A.-L. Cui, Z.-H. Ni, Y.-B. Jiang, L.-F. Zhang, J. Ribas; H.-Z. Kou, *Inorg. Chem*. 2006, **45**, 4883.

(55) Y.-Q. Wang, Q.-X. Jia, K. Wang, A.-L. Cheng, E.-Q. Gao, *Inorg.Chem*. 2010, **49**, 1551.

(56) M.A.M Abu-Youssef; A. Escuer; M.A.S. Goher; F.A. Mautner; R. Vicente, *J. Chem. Soc., Dalton Trans.* 2000, 413.

(57) T.K. Karmakar; G. Aromi; B.K. Ghosh; A. Usman; H.-K. Fun, T. Mallah; U. Behrens; X. Solans; S.K. Chandra, *J. Mater. Chem.* 2006, **16**, 278.

(58) Y.-Q. Wang, Q. Sun, Q. Yue, A.-L. Cheng, Y. Song, E.-Q. Gao, *Dalton Trans*. 2011, **40**, 10966.

(59) A. Das; G.M. Rosair; M.S. El Fallah, J. Ribas; S. Mitra, *Inorg. Chem*. 2006, **45**, 3301.

(60) J.L. Manson; A.M. Arif; J.S. Miller, *Chem. Commun*. 1999, 1479.

(61) J. Cano, E. Ruiz, S. Alvarez, M. Verdaguer, *Comments Inorg. Chem*. 1998, **20**, 27

(62) E. Ruiz, J Cirera, S. Alvarez, *Coord. Chem. Rev*. 2005, **249**, 2649.

(63) A. Schaefer, C. Huber, R. Ahlrichs, *J. Chem. Phys*. 1994, **100**, 5829.

(64) A.D. Becke, *J. Chem. Phys*. 1993, **98**, 5648.

(65) *Gaussian 09 (Revision D01):* M.J. Frisch, G.W. Trucks, H.B. Schlegel, G.E. Scuseria, M.A. Robb, J.R. Cheeseman, G. Scalmani, V. Barone, B. Mennucci, G.A. Petersson, H. Nakatsuji, M. Caricato, X. Li, H.P. Hratchian, A.F. Zmaylov, I.J. Bloino, G. Zheng, J.L. Sonnenberg, M. Hada, M. Ehara, K. Toyota, R. Fukuda, J. Hasegawa, M. Ishida, T. Nakajima, Y. Honda, O. Kitao, H. Nakai, T. Vreven, J.J.A. Montgomery, J.E. Peralta, F. Ogliaro, M. Bearpark. J.J. Heyd, E. Brothers, K.N. Kudin, V.N. Staroverov, R. Kobayashi, J. Normand, K. Raghavachari, A. Rendell, J.C. Burant, S.S. Iyengar, J. Tomasi, M. Cossi, N. Rega, J.M. Millam, M. Klene, J.E. Knox, J.B. Cross, V. Bakken, C. Adamo, J. Jaramillo, R. Gomperts, R.E. Stratmann, O. Yazyev, A.J. Austin, C. Cammi, J.W. Pomelli, R. Ochterski, R.L. Martin, K. Morokuma, V.G.

Zakrzewski, G.A. Voth, P. Salvador, J.J. Dannenberg, S. Dapprich, A.D. Daniels, O. Farkas, J.B. Foresman, J.V. Ortiz, J. Cioslowski, D.J. Fox, C.T. Wallingford, 2009.

(66) I. Seggern, F. Tuczek, W. Bensch; *Inorg. Chem*. 1995, **34**, 5530.

(67) M.-F. Charlot, O. Kahn, M. Chaillet, C. Larrieu, *J. Am. Chem. Soc*. 1986, **108**, 2574.

(68) M.A. Aebersold, M. Gillon, O. Plantevin, L. Pardi, O. Kahn, P. Bergerat, I.F.T. von Seggern, L. Ohrström, A. Grand, E. Lelièvre-Berna, *J. Am. Chem. Soc*. 1998, **120**, 5238.

(69) R. Vicente, A. Escuer, J. Ribas, M.S. El Fallah, X. Solans,M. Font-Bardia, *Inorg. Chem.* 1993, **32**, 1920.

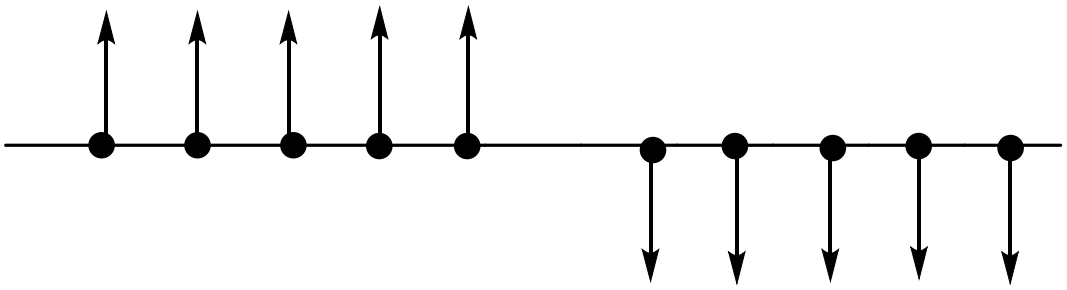

Scheme 1

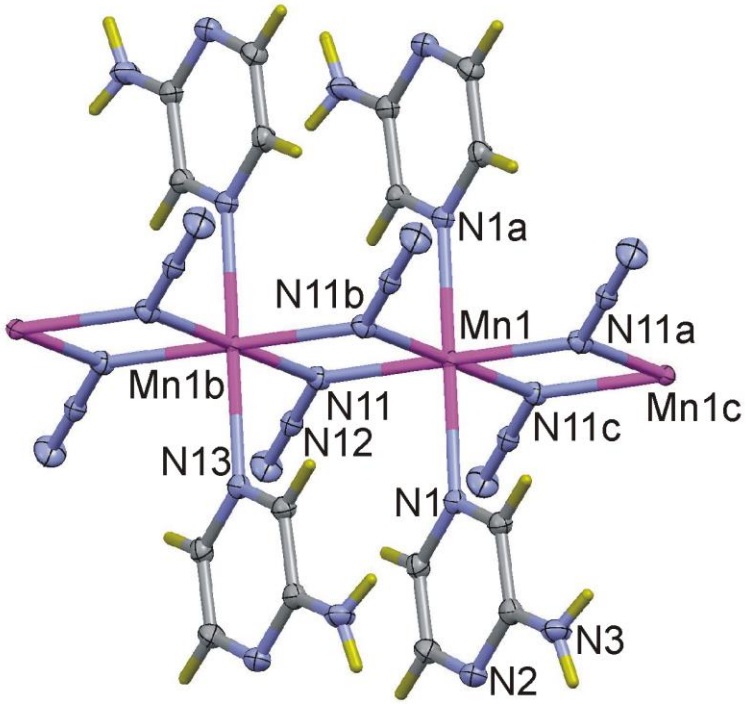

Figure 1a

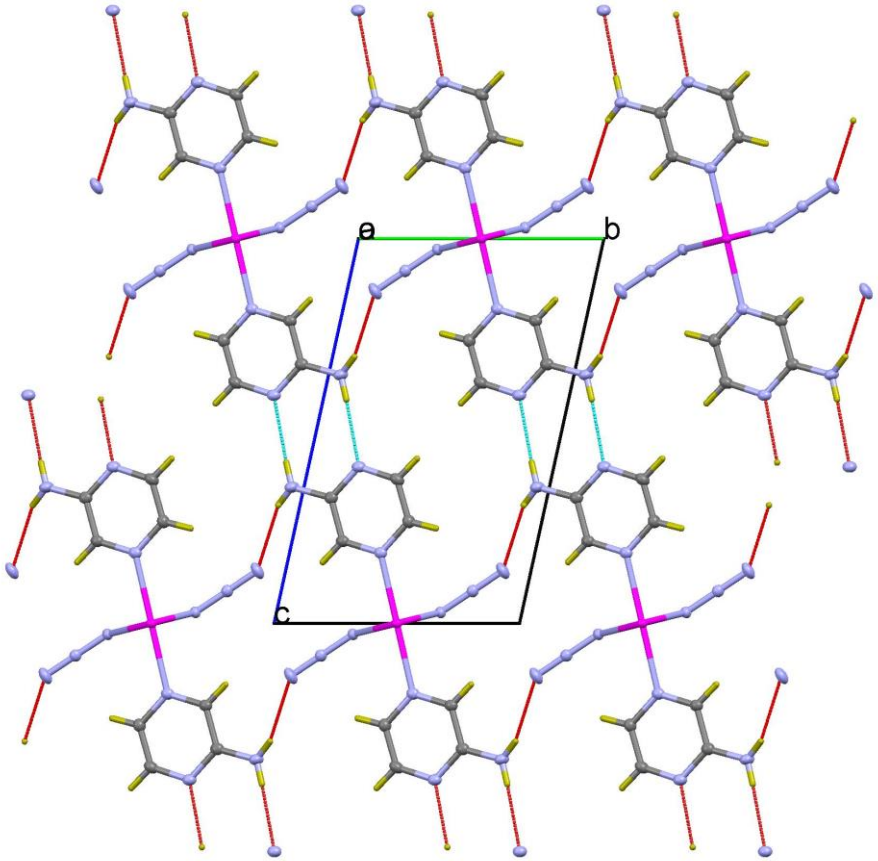

Figure 1b

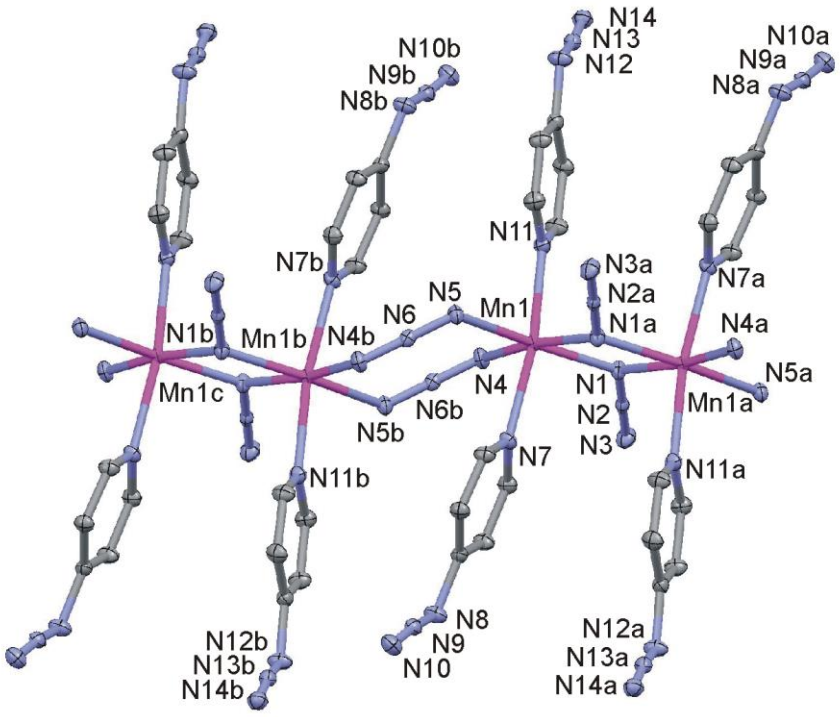

Figure 2a

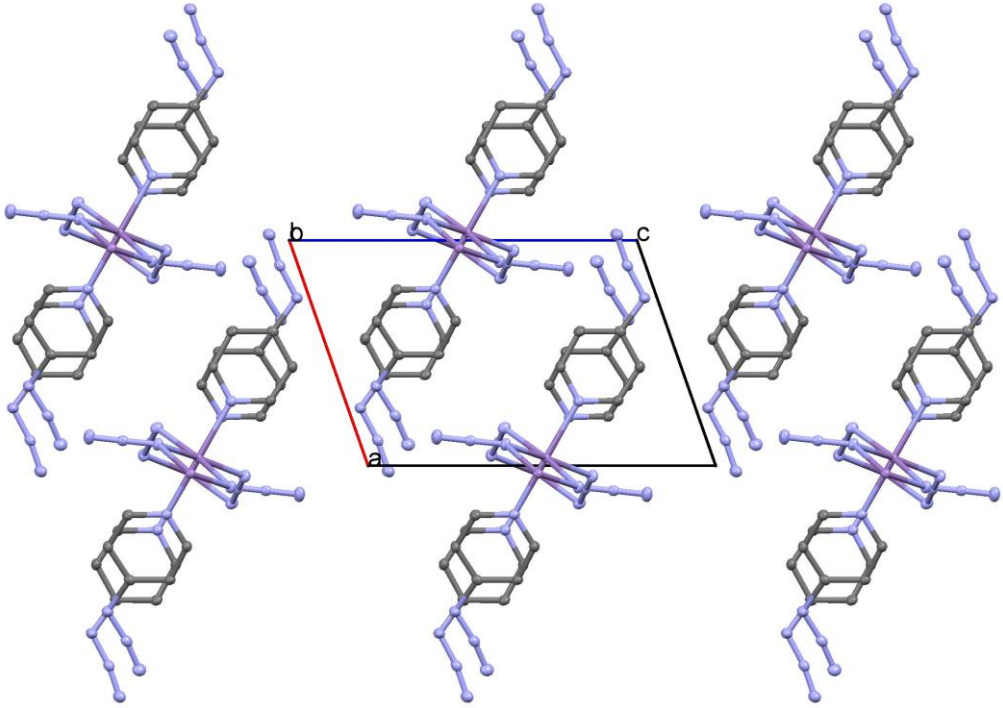

Figure 2b

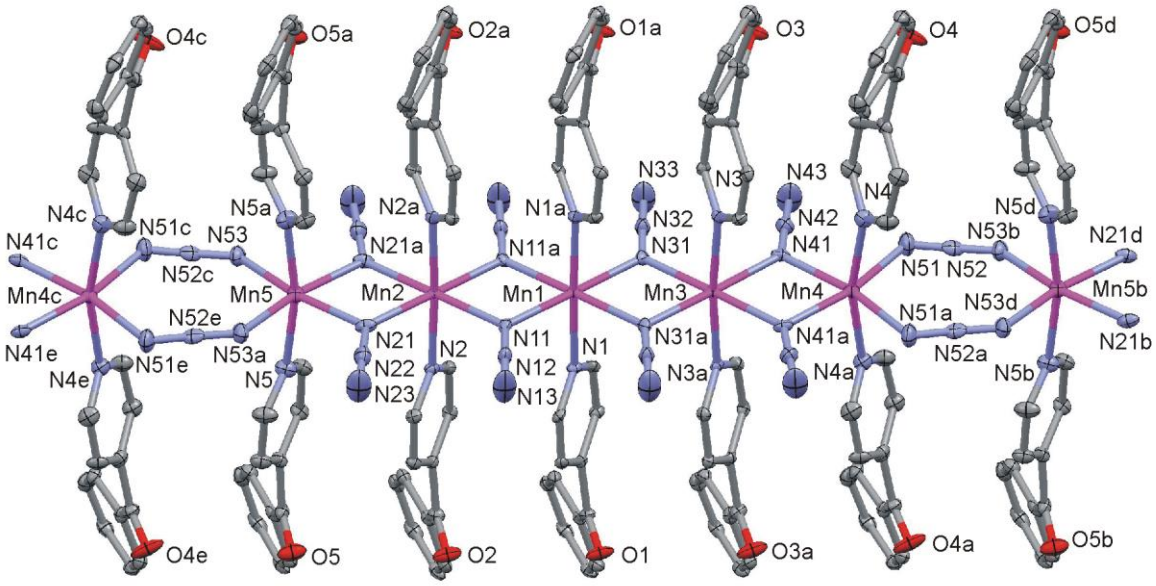

Figure 3a

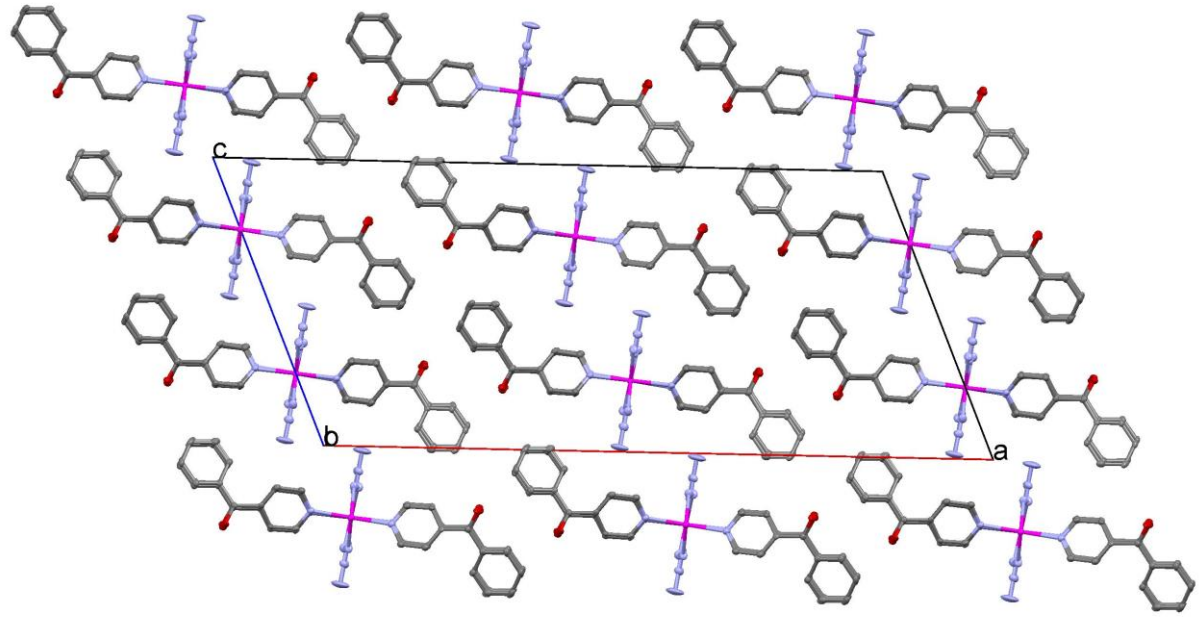

Figure 3b

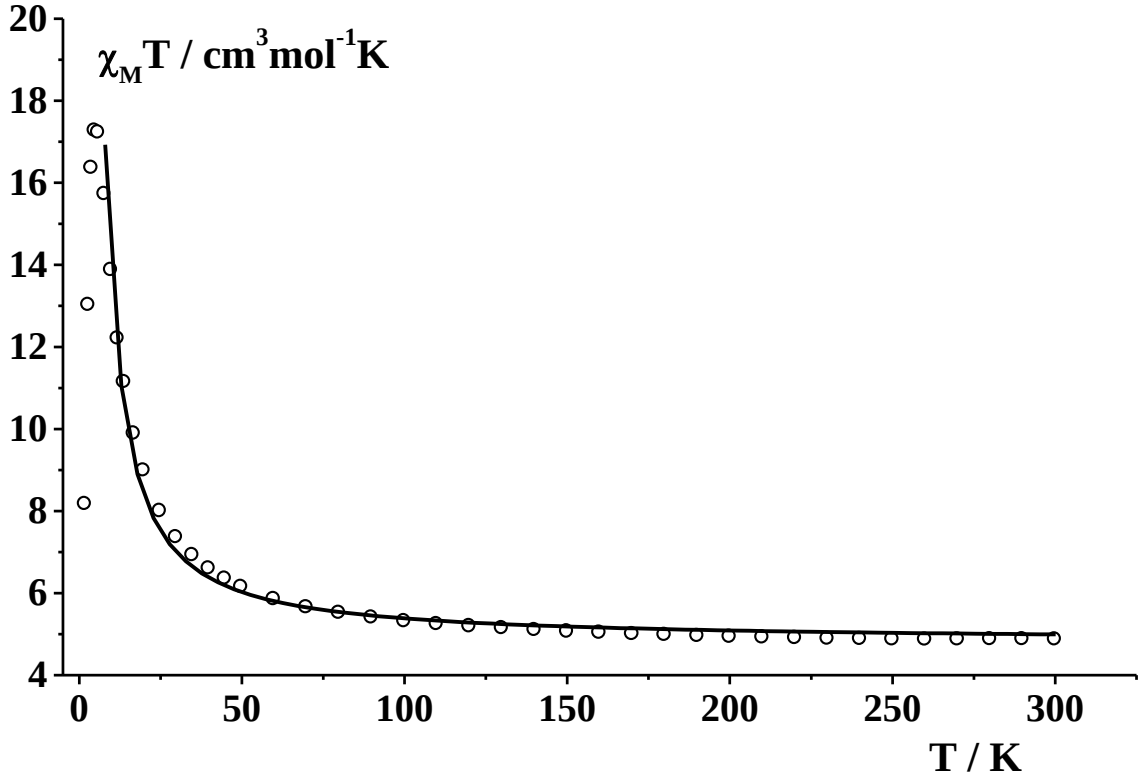

Figure 4

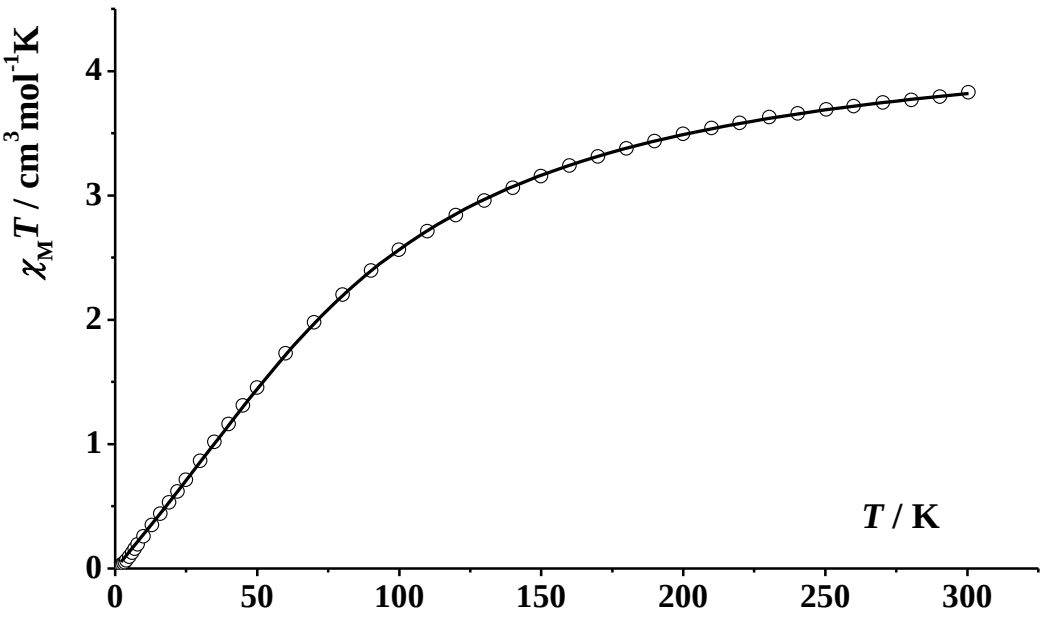

Figure 5

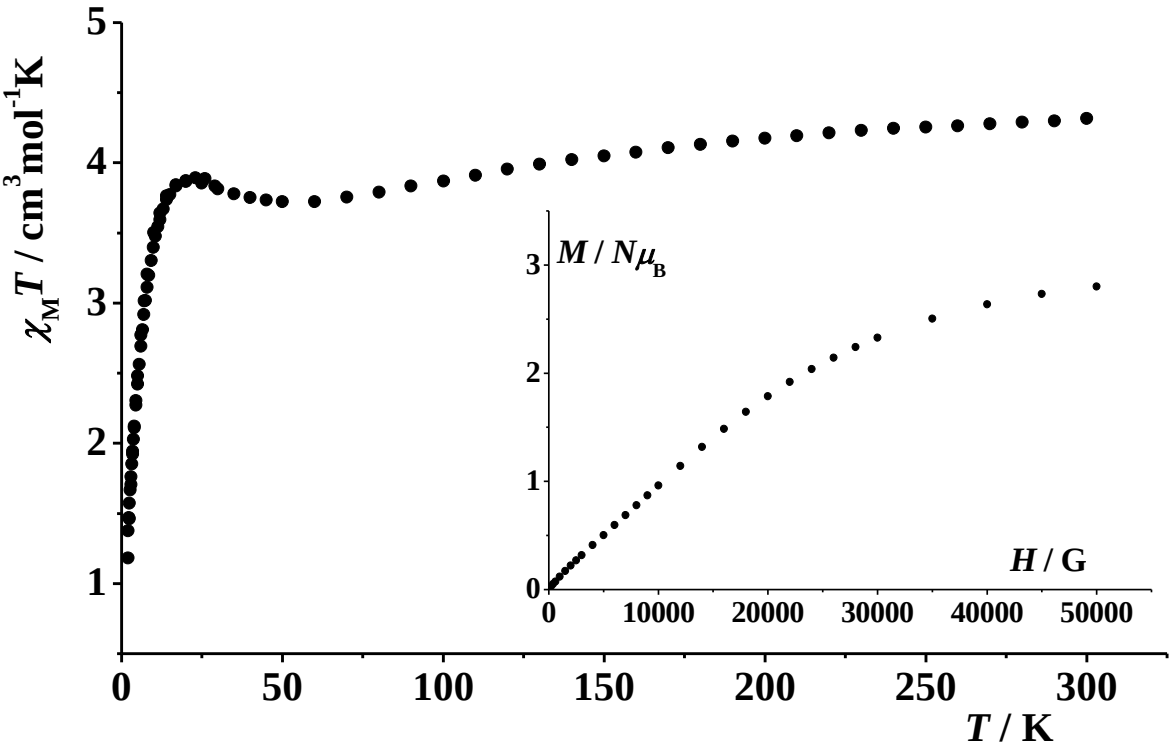

Figure 6

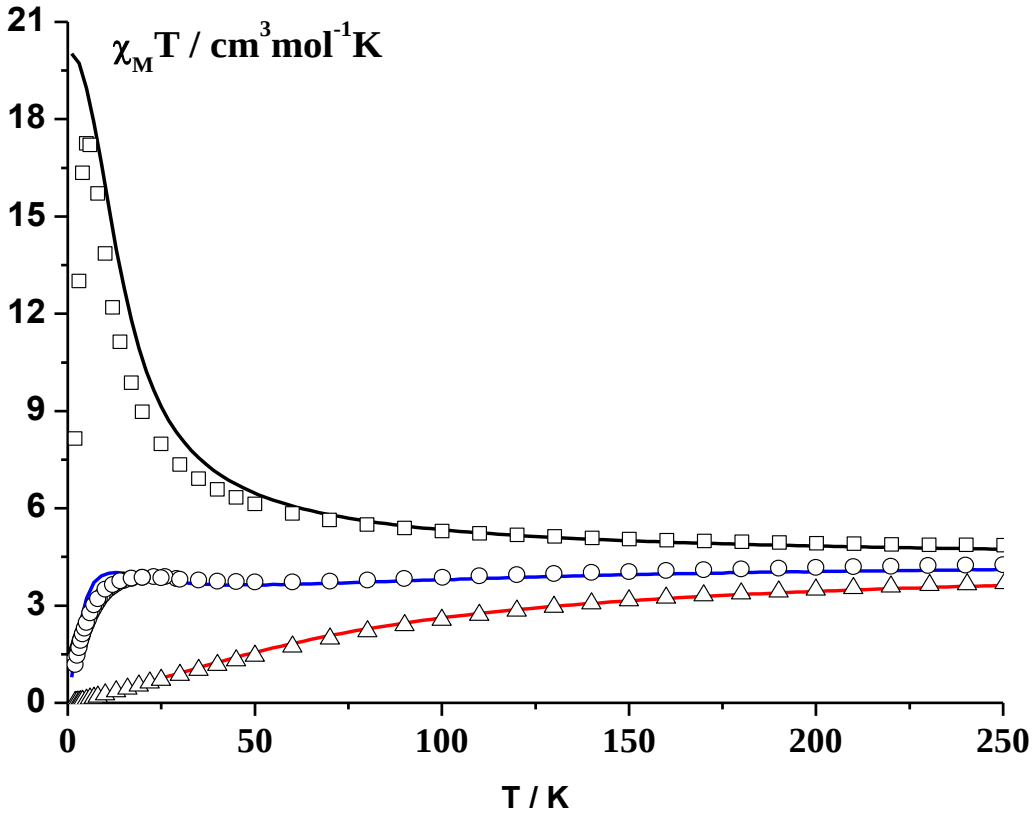

Figure 7

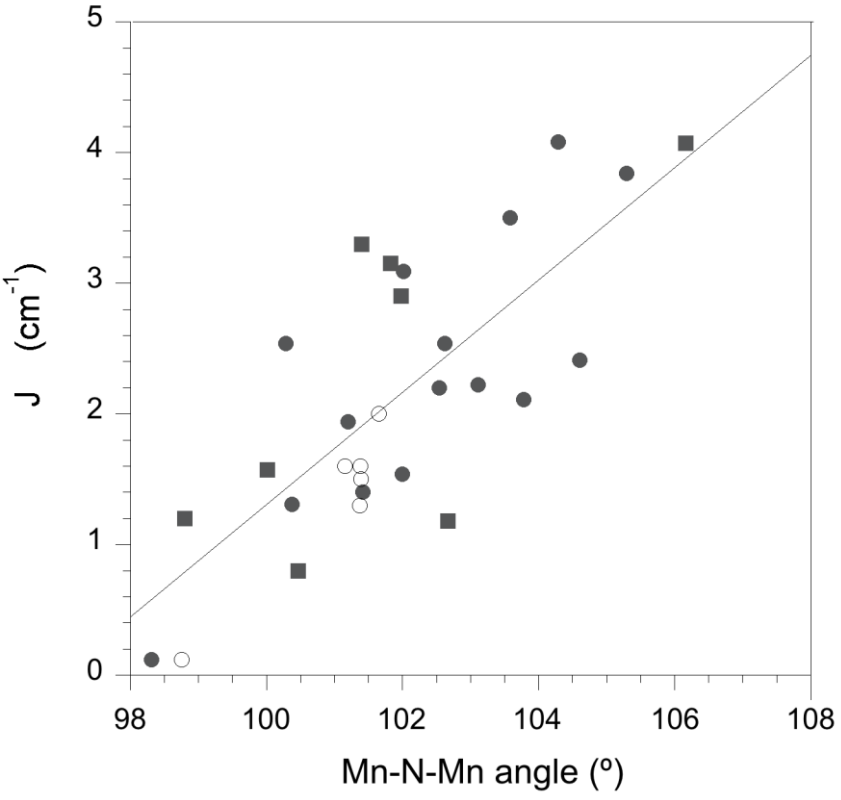

Figure 8

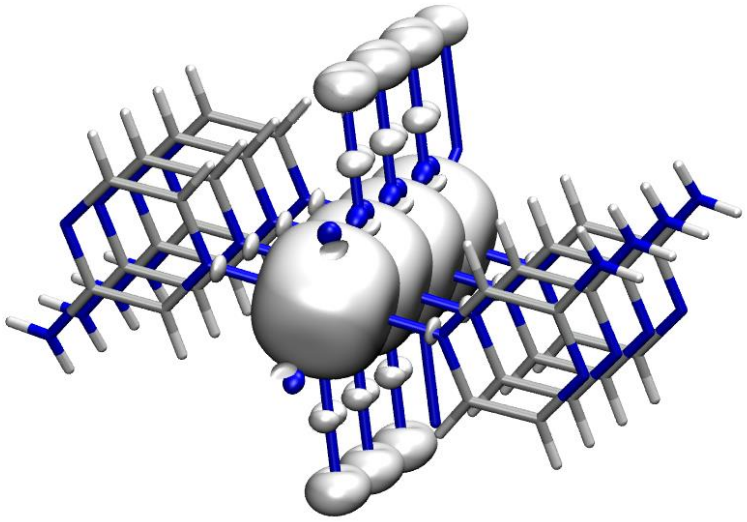

Figure 9